ORIGINAL ARTICLE

Structural and Mechanical Characterization of Duplex Multilayer Coatings Deposited onto H13 Tool Steel

Abel André Candido Recco[1], André Paulo Tschiptschin[2,*]

[1]*Physics Department, Universidade do Estado de Santa Catarina (UDESC), Joinville, Brazil.*
[2]*Metallurgical and Materials Engineering Department, Universidade de São Paulo (USP), São Paulo, Brazil.*

Quenched and tempered H13 tool steel was plasma nitrided and Physical Vapour Deposition (PVD) coated in a hybrid reactor aiming to obtain a TiN/TiC multilayer coating deposited on a plasma nitrided substrate, with a more gentle transition of elastic-plastic properties between the outermost layer of the coating and the substrate. Duplex treatment (plasma nitriding and PVD coating) was carried out in a hybrid reactor. Plasma nitriding preceded the DC triode magnetron sputtering PVD process, conducted inside the same chamber, using CH_4 and N_2 as reactive gases. Multilayer TiN/TiC coatings deposited on a nitrided H13 substrate were obtained. The multilayer coating was composed by a first Ti interlayer to grant adhesion, followed by a second 18.4 at% C TiC layer with a cF8 NaCl type unit cell, then a 41.9 at% N TiN layer and finally an outermost 32.3 at% C TiC layer with the same cF8 NaCl type unit cell. The multilayer coating showed a gentle transition of elastic-plastic properties assessed by the H/E^* and the H^3/E^{*2} ratios and the elastic recovery as a function of the distance from the surface of the specimen. The adhesion of the multilayered coating to the substrate was greater in the case of the duplex coated specimen as compared to the non duplex treated H13 steel.

KEY WORDS: PVD-TiN, PVD-TiC; Plasma nitriding; PVD coating; Multilayer coatings.

1. Introduction

Mechanical systems being designed nowadays operate in ever more severe conditions, sustaining high applied loads, higher temperatures, greater sliding speeds and much more severe environments. The combination of usually conflicting properties is required in order to achieve higher productivity, high power efficiency, low energy consumption, and low levels of emissions. The design of these mechanical systems involves the combination of properties such as low friction, high wear resistance, high load bearing capacity, and fatigue resistance.

When subjected to high intensity loading, a thin coating may collapse, mainly due to substrate elastic and plastic deformation, resulting in premature failure of the coating. For many applications the performance of a coating is limited by the mechanical properties of the substrate material itself. Thin films require a mechanical support given by the substrate material to avoid the so-called 'eggshell effect', granting good adhesion to the hard coating.

Optimization of tribological properties of materials comprises designing coating systems with different architectures, defined by a sequence of deposited coating layers

*Corresponding author.
E-mail address: antschip@usp.br (A. P. Tschiptschin)

that should resist to physical, physical-chemical, and mechanical interactions arisen in service.

Different types of coating structures may be found in today's coating technology: single layer coatings, sandwich coatings, and graded coatings. Most commercial Chemical Vapour Deposition (CVD) and Physical Vapour Deposition (PVD) coatings are made up of one single layer often containing one structure phase. Among the most frequent are TiC, TiN, CrN, alumina (Al_2O_3), and diamond-like carbon (DLC). They are usually applied directly onto the surface of a homogeneous substrate material. Sometimes the monolayer may be constituted by more than one component or by a gradient of compositions with mechanical properties varying accordingly.

Duplex coatings, on the other side, are obtained by combining a surface treatment of the substrate with a coating deposition. Single layer and multilayer coatings can be applied over pre-nitrided or any other diffusion treated surface that modifies the substrate properties in the region close to the coating interface, approximating the properties of the substrate and of the ceramic coating layer[1].

Nanocomposite coatings based on a dispersion of transition metal (TM) nanometric carbides in a carbon amorphous matrix, such as TiC/a-C coating[2], have also been proposed to reduce friction and wear of machine mechanical components. The formation of a nanocomposite structure in amorphous carbon coatings increases the toughness of the material. The combination of an amorphous matrix, in which no dislocation-based deformation mechanisms are possible, due to lack of crystallinity, with a dispersion of hard nanoparticles enhance simultaneously the hardness and toughness of these coatings, while maintaining low sliding friction coefficients[3].

The aim of this work is to characterize the microstructure and the mechanical properties of a duplex multilayered coating deposited onto the surface of a plasma nitrided H13 tool steel.

2. Methods

Quenched and tempered H13 mold tool steel specimens were duplex treated in a hybrid Triode Magnetron Sputtering (TMS) reactor. Plasma nitriding and PVD coating were done inside the same chamber, by changing the processing parameters used for each of the diffusion and coating treatments steps. When duplex treatments are performed in a hybrid reactor, contact of the specimen´s surface with air, between the treatments, is avoided and no cleaning or activating of the pre-nitrided surface is needed. Plasma nitriding was carried out in conditions where no white layer can be formed. After plasma nitriding, PVD coating is carried out, by depositing, at first, a Ti interlayer to grant adhesion of the TiC and TiN layers. After deposition of the Ti interlayer, reactive deposition is carried out when Ti atoms react either with N_2 or CH_4 providing the formation of TiN or TiC coatings. The multilayer architecture constituted by alternating layers of TiC and TiN were obtained by changing the (N_2 + Ar) and (CH_4 + Ar) reactive gases in the plasma atmosphere.

Plasma nitriding was carried out at 520ºC, for 2 hours, in a 95% H_2 + 5% N_2 atmosphere. The 100 nm thick Ti interlayer was deposited during 2 minutes. PVD coatings was performed at 300ºC under −40 VDC bias, 640 W being applied to the cathode; pressure was maintained at 1×10^{-6} Torr and argon partial pressure was 3.0 mTorr. PVD coatings thickness varied from 2.0 to 2.7 μm. Part of the specimens was PVD coated without being plasma nitrided previously. Table 1 shows the nitriding and coating times and thicknesses of the ceramic layers deposited under seven different coating conditions. The TiN*(A3) and TiC*(B3) films were obtained by depositing TiN and TiC onto a non-nitrided H13 substrate. TiN(A3), TiC(B3), and TiC(B2) specimens were duplex coated, the ceramic layers being deposited onto pre-nitride H13 tool steel. The Multilayer-w/o-Nit specimen was coated with a multilayer deposited onto the quenched and tempered H13 steel. The Multilayer-w-Nit specimen was duplex treated, the multilayer coating being deposited over a plasma nitrided substrate.

The coatings were chemically and structurally characterized by X-ray diffraction, Wavelength Dispersive X-ray Spectroscopy (WDX), Raman and X-ray Photoelectron (XPS) Spectroscopy after being deposited onto Si wafers.

Mechanical and tribological properties were assessed via depth sensing and micro-scratch techniques applied to coatings deposited onto the H13 quenched and tempered tool steel.

3. Results and Discussion

3.1 Structural and Chemical Characterization

3.1.1 Ti + N_2 reactive deposition

Fig. 1 shows X-ray diffraction patterns of coatings obtained under four different conditions of (Ti + N_2) reactive depo-

Table 1 Nitriding and coating times and thicknesses of the ceramic layers deposited under seven different coating conditions

Specimen	t_{nit} (h)	Film	t_{dep} (h)	t (μm)
TiN*(A3)	0	TiN	3.2	2.0
TiC*(B3)	0	TiC	3.0	2.1
TiN(A3)	2	TiN	3.0	2.3
TiC (B3)	2	TiC	4.0	2.2
TiC (B2)	2	TiC	2.0	2.4
Multilayer-w/o-Nit	0	TiC(B2)-TiN(A3)-TiC(B3)	4.6	2.7
Multilayer-w-Nit	2	TiC(B2)-TiN(A3)-TiC(B3)	4.6	2.7

TiN* and TiC* are TiN and TiC coatings deposited onto non-nitrided H13 specimens.

sition A1, A2, A3, and A4. Nitrogen atomic contents measured using WDS techniques are also shown. In addition, the metallic Ti diffractogram is also shown for comparison purposes.

The (α-Ti) peak shows up in all diffractograms as the metallic Ti interlayer deposited prior to the reactive sputtering is detected.

Increasing the nitrogen flux and nitrogen partial pressure, during deposition, leads to greater nitrogen contents in the film. When the nitrogen over argon flux ratio $F_{reactive}/F_{Ar}$ increases from 0.05 to 0.1, the nitrogen content changes from 16.8 at.% to 39.2 at.%. Nevertheless, increasing the $F_{reactive}/F_{Ar}$ ratio from 0.1 to 0.4 leads to a very low change of the nitrogen content from 39.2 at.% to 43.3 at.%.

The maximum nitrogen equilibrium content in (α-Ti) at 300°C, calculated using Thermocalc, is approximately 10 at.%. The sputtering process is typically a non-equilibrium one and supersaturated metastable (α-Ti) with 16.8 at.% N in solution is obtained. The α-Ti (002) peak is shifted to the left due to nitrogen supersaturation at the octahedral sites of the hexagonal unit cell.

TiN with a cF8 NaCl unit cell forms for the A2, A3, and A4 conditions. The film texture changed for the A3 deposition, the (111) orientation turning out to be very strong.

3.1.2 Ti + CH$_4$ reactive deposition

The increase of the methane flux and methane partial pressure for the Ti + CH$_4$ reactive deposition leads to greater carbon contents (measured by XPS) in the film as shown in Fig. 2.

The maximum solubility of carbon in (α-Ti) at 300°C is 0.07 at.% according to Thermocalc. The (Ti + CH$_4$) reactive deposition using B1 condition leads to the formation of supersaturated hexagonal (α-Ti) containing 10.8 at.% of carbon. For the B2 and B3 conditions, 18.4 at.% and 32.3 at.% of carbon are dissolved in the cF8 NaCl type TiC phase, respectively. A slight shift of the (111) plane to lower 2θ val-

ues can be attributed to changes in chemical composition and stress states of the TiC films[4]. The B3 condition leads to a buildup of a strong (111) texture.

For the B4 reactive deposition condition only α-Ti peaks were detected, originated in the Ti interlayer beneath. No TiC diffraction peaks were detected, probably due to a very low TiC volume fraction and a very small crystallite size, of the order of nanometers. B4 reactive deposition led to formation of a coating containing 81.9 at.% of carbon.

Raman and XPS spectra taken from B4 film are shown in Figs. 3 and 4.

O-C=O and C-O structures indicate the presence of surface oxide layers, 3-4 nm thick. aC:H phase was detected both by XPS and Raman spectroscopy. In the Raman spectrum two asymmetric peaks were observed: the first one at 1,580 cm^{-1}, known as G (Grafitic, sp^2), indicating graphitic distorted planes, and the second one at 1,345 cm^{-1}, known
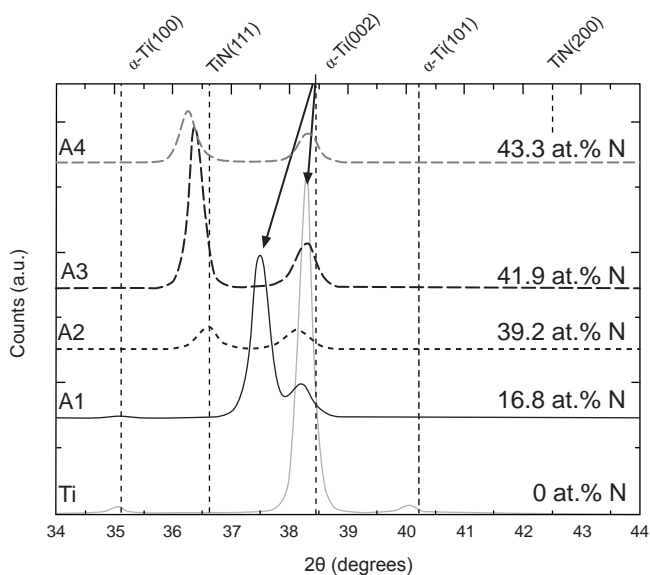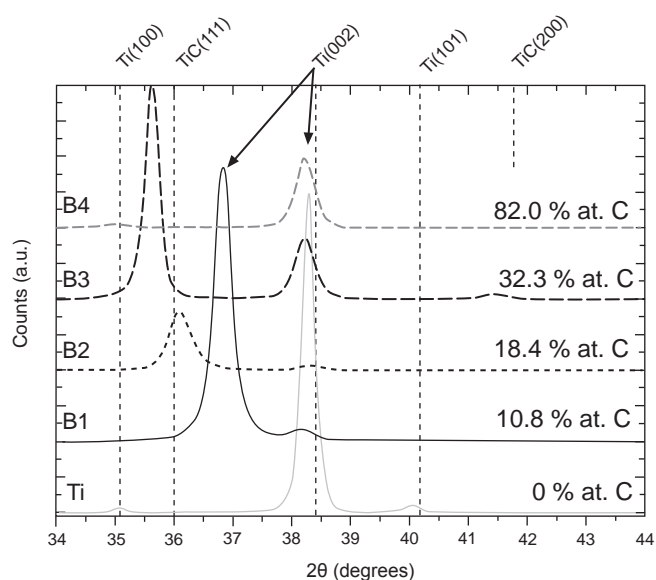

Fig. 2 X-ray diffraction patterns of four different films obtained under different conditions of (Ti + CH4) reactive deposition B1, B2, B3, and B4. The CH$_4$ content in the sputtering gas increases from B1 to B4

Fig. 1 X-ray diffraction patterns of four different films obtained under different conditions of (Ti + N$_2$) reactive deposition A1, A2, A3, and A4. The N$_2$ content in the sputtering gas increases from A1 to A4
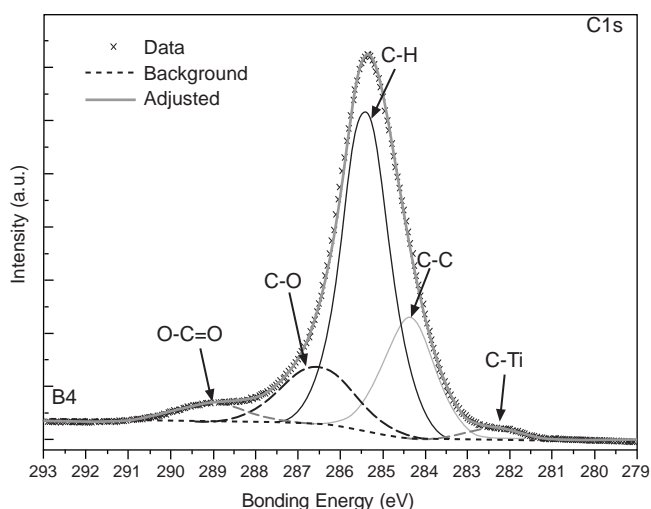

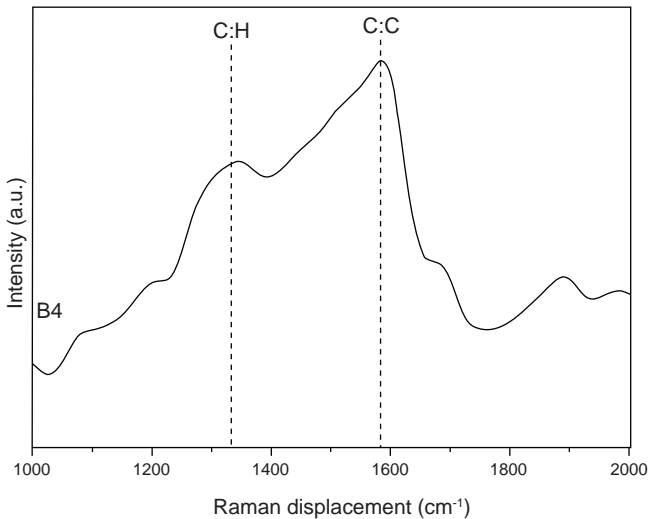**Fig. 3** XPS spectrum of the TiC/a-C:H film obtained in the B4 condition

Fig. 4   514.5 nm laser wavelength Raman spectrum of the B4 coating

as D (Disorder, sp^2-sp^3), usually attributed to disorder created by sp^3 bonding in the aC:H phase.

C-H structures with a 284.6 eV bonding energy and C-Ti with a 281.8 eV bonding energy were observed in the XPS spectrum, indicating the formation of a mixture of amorphous plus crystalline phases in the B4 film. Most probably an amorphous hydrogenated carbon phase matrix containing very small crystals of TiC was formed.

Fig. 5 shows that increasing methane content in reactive gas increases Ti-C/Ti ratio from 0.14 to 0.27, 0.43, and 0.49 for the B1, B2, B3, and B4 conditions and shifts X-ray diffraction peaks to the left, indicating that more carbon atoms occupy octahedral interstice sites of TiC unit cell. In Fig. 5 peaks of Ti-O appear corresponding to the titanium oxide formed on the surface of the specimen.

The ratio of TiC to the amorphous aC:H phase, not taken into account the presence of oxygen, was calculated and found to be 0.11 for the B4 condition. For the other three conditions no formation of hydrogenated carbon amorphous phase was detected. The formation of the aC:H amorphous
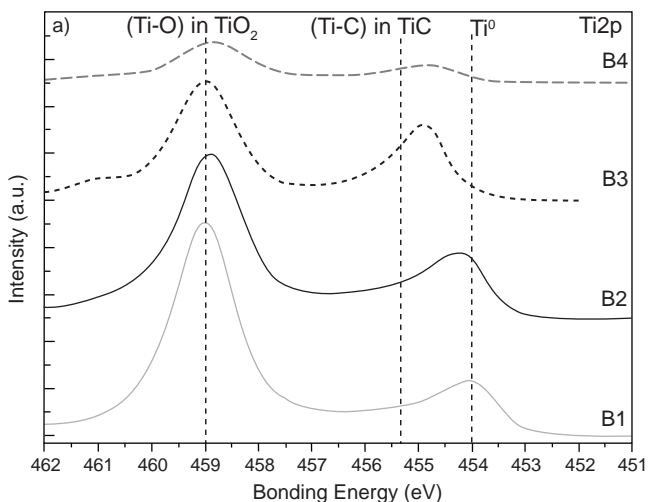
phase is favored by greater amounts of methane in the reactive gas, probably due to a more intense target poisoning effect of the CHx species[5,6].

In the Ti-C system, three phases coexist: the C supersaturated Ti, TiC compound, and an excess carbon phase. Kim et al.[7] discuss the formation of TiC compound as a function of free energy wells of supersaturated Ti, TiC, and C bound phases in the Ti-C system: in comparison with the TiN coating process, the coating parameters of the TiC deposition process are relatively more sensitive to the composition ratio of methane in the reactive gas.

3.2 Micromechanical Characterization

Adhesion of the films to the substrate was assessed using the Rockwell C and micro-scratch adhesion tests.

3.2.1 Adhesion of monolayer films deposited onto H13 tool steel

3.2.1.1 Monolayer films

Table 2 summarizes the mechanical properties, measured by depth-sensing techniques, of the monolayer films deposited onto non-nitrided and pre-nitrided quenched and tempered H13 tool steel. TiN(A3) and TiN(B3) films show hardness around 30 GPa and Young modulus around 280 GPa, although the B3 film deposited onto the pre-nitrided specimen showed a Young modulus a little bit lower (260 GPa).

Hardness and Young modulus of the non-nitrided and pre-nitrided quenched and tempered H13 tool steel were also measured. It was obtained H_{H13} = 7.2 ± 0.9 GPa and Y_{H13} = 202 ± 4.7 GPa, respectively, and hardness on top of the nitrided layer and Young modulus on top of the nitrided H13 tool steel H_{NIT} = 14.3 ± 0.4 GPa and H_{NIT} = 220 ± 3.6 GPa, respectively.

Table 3 shows the results of Rockwell C and micro-scratch adhesion tests. The quality indexes HF of the surface around the indentation, for the TiN*(A3) and TiC*(B3), deposited onto non-nitrided quenched and tempered H13 were poor, namely HF4 and HF5. The TiN(A3), TiC(B3), and TiC(B2) coatings deposited onto the plasma pre-nitrided

Fig. 5   Ti2p XPS spectra of different films obtained for B1, B2, B3, and B4 conditions and increasing methane contents um the gas

Table 2   Mechanical properties of monolayer films deposited onto non-nitrided and pre-nitrided quenched and tempered H13 tool steel

Specimen	H(GPa)	E*(GPa)[1]	Film	t (μm)
TiN*(A3)[2]	28.6 ± 1.6	283.8 ± 8.5	TiN	2.0
TiC*(B3)[2]	33.7 ± 1.4	259.9 ± 5.0	TiC	2.1
TiN(A3)	30.6 ± 1.2	280.3 ± 6.8	TiN	2.3
TiC (B3)	38.2 ± 1.0	287.8 ± 3.5	TiC	2.2
TiC (B2)	17.9 ± 0.7	193.0 ± 4.8	TiC	2.4

[1]The reduced Young modulus E* was assessed using the Hertz equation, $\dfrac{1}{E^*} = \dfrac{(1-v_i^2)}{E_i} + \dfrac{(1-v_{film}^2)}{E_{film}}$, where E_i and v_i correspond to the mechanical properties of the indenter.

[2]TiN* and TiC* are TiN and TiC coatings deposited onto non-nitrided H13 specimens.

Table 3 Rockwell C and scratch test adhesion tests of monolayer films deposited onto non-nitrided and pre-nitrided quenched and tempered H13 tool steel

Specimen	HF	L_{C1} (N)	L_{C2} (N)
TiN*(A3)	4	4.5 ± 0.5	15.3 ± 2.4
TiC*(B3)	5	2.7 ± 2.0	8.4 ± 2.2
TiN(A3)	1	36.4 ± 2.1	54.0 ± 4.8
TiC(B3)	1	5.8 ± 2.4	11.6 ± 1.6
TiC(B2)	1	13.9 ± 1.0	24.1 ± 2.3

*Stands for TiN and TiC coatings deposited onto non-nitrided H13 specimens.

specimens showed a very good quality index HF1. The results obtained in the Rockwell C adhesion tests show the significant role that the plasma nitrided layer plays by increasing the load bearing capacity of the substrate[1,6]. Nevertheless, this technique cannot differentiate the adhesion of the monolayer films TiN(A3), TiC(B2) and TiC(B3) deposited onto the pre-nitrided steel. The Rockwell C adhesion test is strongly dependent on the substrate hardness and film thickness as discussed by Ollendorf *et al*.[8].

The critical loads for formation of the first cracks in the ceramic films (L_{C1}) and for delamination of the film (L_{C2}) in the scratch test, corresponding, respectively to cohesive and adhesive failures, are also shown in Table 3. Once again, one can see that the non-nitrided specimens show very low L_{C1} and L_{C2} critical loads while for the pre-nitrided specimens the critical loads are much greater. It is worth noting that the TiC*(B3) coating, deposited onto the non-nitride H13 steel, showed a high quality index HF1 but did not behave in the same manner during the scratch test, the L_{C1} and L_{C2} critical loads being smaller than the ones obtained for the duplex treated specimens.

Table 4 shows the elastic recovery (W_e), and the resistance to elastic (H/E^*) and plastic (H^3/E^{*2}) deformation of the ceramic films, obtained in the indentation tests. The TiN(A3) and TiC(B2) ceramic films, deposited onto the nitrided H13 steel specimens, show the same elastic recovery (57%) and H/E^* ratios (0.1), although their resistance to plastic deformation (H^3/E^{*2}) are quite different.

The TiC(B2) and the substrate undergo elastic-plastic deformation and the adhesive failure is mainly determined

by the low resistance of the TiC(B2) film to plastic deformation.

When comparing films with different H^3/E^{*2} ratios and quite same elastic recoveries (58%) and H/E^* ratios, deposited onto substrates with similar elastic-plastic properties, one can see that increasing the resistance to plastic deformation (H^3/E^{*2}) of the film increases the adhesion of the film to the substrate, as seen for the TiN(A3) film deposited onto pre-nitrided H13 steel. Besides the effect of the increase in the load bearing capacity of the substrate, the increase in the resistance to plastic deformation of the film plays an important role for improving the adhesion.

TiN(A3) and TiN*(A3) films show the same elastic recoveries, same H/E^* ratios, and same resistance to plastic deformation (H^3/E^{*2}). In this case only the greater load bearing capacity of the substrate was decisive to increase the adhesion. The observed loss of adhesion can be attributed to an egg shell effect as proposed by Nix *et al*.[9]. The same behavior was observed for TiC(B3) and TiC*(B3) films deposited onto nitrided and non-nitrided H13 substrates, respectively.

No improvement of adhesion of the TiC(B3) film, deposited onto pre-nitrided H13 specimens, was observed, despite the greater load bearing capacity of the nitrided substrate. In this case the determining factor of this behavior is the great difference between the elastic-plastic properties of the film and the substrate. The increase in hardness granted by the plasma nitriding treatment was not sufficient to reach hardness values near 38 GPa, as reported in Table 2, for TiC(B3) film.

Plasma nitriding of H13 substrate appears to be useful to increase the adhesion of deposited TiN films. On the other hand, the nitriding treatment did not show any beneficial effect on the adhesion properties of TiC ceramic films.

3.2.2 Adhesion of the multilayer coating onto H13 tool steel

Based on the supposition that a more gentle transition of elastic-plastic properties of the layers in the film can improve the adhesion to the substrate, an attempt was made to obtain a functionally graded multilayer film, with smaller differences of elastic-plastic properties. The H/E^* and H^3/E^{*2} ratios and the elastic recovery were gradually increased, by choosing an appropriate sequence of deposition and corresponding deposition processes.

Table 4 Critical loads, elastic recovery, H/E^* and H^3/E^{*2} ratios for the ceramic films and the H13 tool steel

Specimen	L_{C1} (N)	L_{C2} (N)	w_e (%)	$H/E^* \times 10^{-2}$	H^3/E^{*2} (GPa)
TiN(A3)	36.4 ± 2.1	54.0 ± 4.8	59 ± 2	10.9 ± 0.5	0.36 ± 0.05
TiC(B2)	13.9 ± 1.0	24.1 ± 2.3	57 ± 2	9.3 ± 0.4	0.15 ± 0.05
TiN*(A3)	4.5 ± 0.5	15.3 ± 2.4	55 ± 2	10.0 ± 0.4	0.29 ± 0.06
TiC(B3)	5.8 ± 2.4	11.6 ± 1.6	77 ± 1	13.3 ± 0.4	0.68 ± 0.06
TiC*(B3)	2.7 ± 2.0	8.4 ± 2.2	80 ± 1	13.0 ± 0.3	0.57 ± 0.08
H13 pre-nitrided	—	—	43 ± 2	6.5 ± 0.2	0.06 ± 0.01
H13 non-nitrided	—	—	24 ± 3	3.5 ± 0.3	0.03 ± 0.01

*Stands for TiN and TiC coatings deposited onto non-nitrided H13 specimens.

The 2.7 μm thick multilayer film is composed initially by a 100 nm thick metallic Ti interlayer to improve adhesion, followed by a 18.4 at% C TiC(B2) layer with 0.6 μm and then by a 0.8 μm thick TiN(A3) layer. The outermost layer 1.0 μm thick is a 32.3 at% C TiC(B3) film. Fig. 6 shows the structure of the multilayer film deposited onto the nitrided H13 tool steel.

Vancoille et al.[10] obtained a multi-layer TiC/ Ti(C,N)/TiN coating deposited onto a high-speed steel substrate. The coating thickness was 2 μm and up to nine distinct sublayers could be observed. The composition also changed gradually from TiC at the surface to TiN at the interface.

Table 5 shows the results of the Rockwell C and microscratch adhesion tests for the multilayer films. The result for the TiN*(A3) is also shown for comparison purposes.

The critical load for cohesive failure of the multilayer coatings did not show any significant increase over the critical loads observed for the TiN(A3) condition. The increase of the load bearing capacity of the substrate did not have any significant influence over the L_{C1} critical load for cohesive failure.

Yasuoka et al.[11] studied the mechanical and tribological behavior of TiC/TiC$_{0.5}$N$_{0.5}$/TiN multilayer coating deposited onto High Speed Steel, concluding that the TiC$_x$N$_{1-x}$ crystal lattice parameter moves from TiN to TiC as the carbon ratio increases, and the replacement of N by C could give rise to the lattice strain. The multilayer coating demonstrated higher hardness than the other coatings between 200 mN and 500 mN indenter loads. The multilayer coating exhibited similar, though slightly lower, hardness plastic to the TiC$_x$N$_{1-x}$ coating with regard to elastic recovery. Overall, the mechanical performance of the multilayer coating was found to be stronger than the single-layer coating.
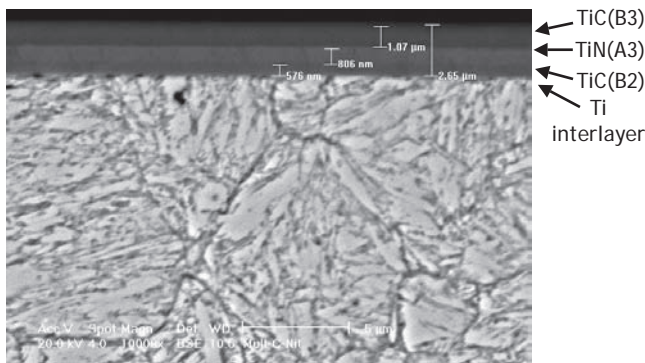

Fig. 6 SEM image of the multilayer film deposited onto pre-nitrided AISI H13 steel

Table 5 Rockwell C and micro-scratch adhesion tests for multilayer films deposited onto non-nitride and pre-nitrided H13 tool steel substrates

Specimen	HF	L_{C1} (N)	L_{C2} (N)
Multilayer-w/o-Nit	1	6.9 ± 2.3	16.7 ± 1.4
Multilayer-w-Nit	1	8.8 ± 0.5	28.8 ± 4.4
TiN*(A3)	4	4.5 ± 0.5	15.3 ± 2.4

*Stands for TiN coating deposited onto non-nitrided H13 specimens.

Similarly, Chen et al.[12] observed that the hardness of TiN/Ti(C,N) multilayer coating is increased due to interface hardening. The adhesion value of TiN/Ti(C,N) multilayer coating is better than that of the Ti(C,N) monolayer coating because the interfaces between TiN and Ti(C,N) layer relax the stress during coating deformation.

Plasma nitriding had an evident beneficial effect on the L_{C2} critical load for adhesive failure. The multilayer film deposited onto the nitrided H13 steel showed the same L_{C2} value shown by the TiC(B2) deposited onto the same substrate. Despite this result, the gradual change of elastic-plastic properties of the multilayer films did not yield greater L_C critical loads for failure when compared to the TiN(A3) monolayer film deposited onto nitrided H13 specimens.

These results point out the important role the innermost layer TiC(B2), with its low H^3/E^{*2} ratio, plays in increasing the adhesion to the substrate. The critical loads observed in this case were very similar to those obtained for the monolayer film TiC(B2). Instead of assuring low friction and greater wear resistance to the coating, in the position of the outermost layer, the 'soft' TiC(B2) transition layer granted grading functionality to the multilayer coating.

Although it is not usual to compare the results of adhesion between different films deposited on various substrates using different deposition techniques, some results regarding adhesion of multilayer coatings published by Chen et al.[12] and Lee[13] are given. Lee compared TiN and CrN monolayer coatings with TiN/CrN multilayer coating deposited onto pre-nitrided quenched and tempered H13 tool steel. The duplex TiN/CrN multilayer coating showed the highest critical load L_C = 43 N compared to the single layer coatings CrN and TiN, which showed critical loads L_C = 24 N and L_C = 38 N, respectively. Chen et al.[12] compared the adhesion behavior of TiCN monolayer coating deposited by magnetron sputtering onto WC-6%Co cemented carbide with a TiN/TiCN multilayer coating deposited by the same technique onto the same tool material, obtaining critical loads L_C = 53 N and 85 N, respectively.

4. Conclusions

DC magnetron sputtering allowed obtaining nitrogen or carbon supersaturated α-Ti, TiN, TiC, or aC:H/TiC nanocomposite.

Nitrogen or carbon supersaturated α-Ti films were obtained using low reactive gas fluxes in the sputtering gas. ac:H/TiC nanocomposite was obtained using high methane flux in the sputtering gas.

B4 and B3 films showed good combination of mechanical properties with high hardness (15 GPa), low reduced Young moduli (140 GPa), and high elastic recoveries (74%), derived from microstructures composed by a combination of amorphous and nanocrystalline phases presented in the microstructure.

Different metallic, ceramic, and composite films were obtained with hardness varying from 11 GPa to 38 GPa, reduced Young moduli varying from 138 GPa to 295 GPa, H/E* ratios from 0.067 to 0.133, H^3/E^{*2} ratios from 0.048 GPa to 0.67 GPa, and elastic recovery varying from 43% to 77%.

A functionally graded coating with a smooth variation of mechanical properties could be obtained by depositing an

engineered sequence of TiN and TiC films onto nitrided and non-nitrided H13 tool steel specimens.

Adhesion tests showed that the adhesion of the single layer to the substrate is very low for films deposited onto non-nitrided H13 tool steel. The quality indexes, obtained in the Rockwell C test, were HF4 and HF6.

The duplex treatment did not assure a good adhesion of TiC ceramic films due to great differences of mechanical properties between the film and the substrate.

The Rockwell C adhesion test could not be used to rank the adhesion behavior of multilayer films deposited onto non-nitrided and pre-nitrided H13 steel. Both showed a quality index HF1.

The TiC(B2) film and the multilayer coating showed similar L_{C2} critical loads, 24 N and 28 N, respectively. The low resistance of the innermost TiC(B2) film to plastic deformation led to similar values of the L_{C2} critical loads in the two coatings.

Acknowledgements

References

1. Sun Y, Bloyce A, Bell T. Finite element analysis of plastic deformation of various TiN coating/substrate systems under normal contact with a rigid sphere. Thin Solid Films 1995; 271(1-2):122-31.

2. Voevodin AA, Prasad SV, Zabinski JS. Nanocrystalline carbide/amorphous carbon composites. J Appl Phys 1997; 82(2):855-8.

3. Pei YT, Galvan D, De Hosson JThM. Nanostructure and properties of TiC/a-C:H composite coatings. Acta Mater 2005; 53(17):4505-21.

4. Inoue S, Wada Y, Koterazawa K. Deposition of TiC films by dual source dc magnetron sputtering. Vacuum 2000; 59(2-3):735-41.

5. Kulikovsky V, Kuzmichev A, Bohac PT, Hubicka Z, Jurek K, Jastrabik L. Composition of Ti-C:H films obtained by pulsed and continuous magnetron sputtering. Surf Coat Technol 2005; 200(1-4):620-4.

6. Recco AAC, Oliveira IC, Massi M, Maciel HS, Tschiptschin AP. Adhesion of reactive magnetron sputtered TiN*x* and TiC*y* coatings to AISI H13 tool steel. Surf Coat Technol 2007; 202(4-7):1078-83.

7. Kim DJ, Cho YR, Lee MJ, Hong JM, Kim YK, Lee KH. Properties of TiN-TiC multilayer coatings using plasma-assisted chemical vapor deposition. Surf Coat Technol 1999; (116-119):906-10.

8. Ollendorf H, Schneider D. A comparative study of adhesion test methods for hard coatings. Surf Coat Technol 1999; 113(1-2):86-102.

9. Nix WD, Bhattacharya AK. Analysis of elastic and plastic deformation associated with indentation testing of thin films on substrates. Int J Solids Struct 1988; 24(12):1287-98.

10. Vancoille E, Celis JP, Roos JR. Tribological and structural characterization of a physical vapour deposited TiC/Ti(C,N)/TiN multilayer. Tribol Int 1993; 26(2):115-9.

11. Yasuoka M, Wang P, Murakami R. Comparison of the mechanical performance of cutting tools coated by either a TiC_xN_{1-x} single-layer or a $TiC/TiC_{0.5}N_{0.5}/TiN$ multilayer using the hollow cathode. Surf Coat Technol 2012; 206:2168-72.

12. Chen L, Wang SQ, Zhou SZ, Li J, Zhang YZ. Microstructure and mechanical properties of Ti(C,N) and TiN/Ti(C,N) multilayer PVD coatings. Int J Refract Met Hard Mater 2008; 26(5):456-60.

13. Lee SY. Mechanical properties of $TiN_x/Cr_{1-x}N$ thin films on plasma nitriding-assisted AISI H13 steel. Surf Coat Technol 2005; 193:55-9.